AD-A146 972 THE ROLE OF FINITE PARALLEL LENGTH ON THE STABILITY OF BARIUM CLOUDS(U) NAVAL RESEARCH LAB WASHINGTON DC J L SPERLING ET AL. 08 NOV 84 NRL-MR-5436 1/1

UNCLASSIFIED F/G 4/1 NL

END

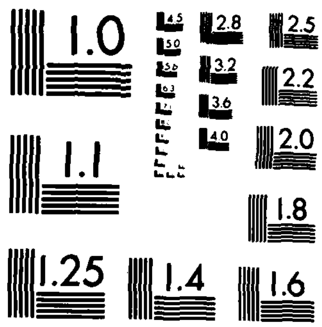
1.0
1.1
1.25
1.4
1.6
1.8
2.0
2.2
2.5
2.8
3.2
3.6
4.0

2

NRL Memorandum Report 5436

The Role of Finite Parallel Length on the Stability of Barium Clouds

J. L. SPERLING,* J. F. DRAKE,†
S. T. ZALESAK AND J. D. HUBA

Geophysical and Plasma Dynamics Branch
Plasma Physics Division

**JAYCOR, Inc.*
San Diego, CA 92138

†Science Applications, Inc.
McLean, VA 22102

November 8, 1984

This research was sponsored by the Defense Nuclear Agency under Subtask S99QMXBC, work unit 00102 and work unit title "Plasma Structure Evolution."

NAVAL RESEARCH LABORATORY
Washington, D.C.

SECURITY CLASSIFICATION OF THIS PAGE

REPORT DOCUMENTATION PAGE

1a REPORT SECURITY CLASSIFICATION UNCLASSIFIED	1b RESTRICTIVE MARKINGS
2a SECURITY CLASSIFICATION AUTHORITY	3 DISTRIBUTION / AVAILABILITY OF REPORT Approved for public release; distribution unlimited.
2b DECLASSIFICATION / DOWNGRADING SCHEDULE	
4 PERFORMING ORGANIZATION REPORT NUMBER(S) NRL Memorandum Report 5436	5 MONITORING ORGANIZATION REPORT NUMBER(S)
6a NAME OF PERFORMING ORGANIZATION Naval Research Laboratory; 6b OFFICE SYMBOL (If applicable) Code 4780	7a NAME OF MONITORING ORGANIZATION
6c ADDRESS (City, State, and ZIP Code) Washington, DC 20375-5000	7b ADDRESS (City, State, and ZIP Code)
8a NAME OF FUNDING / SPONSORING ORGANIZATION Defense Nuclear Agency; 8b OFFICE SYMBOL (If applicable) RAAE	9 PROCUREMENT INSTRUMENT IDENTIFICATION NUMBER
8c ADDRESS (City, State and ZIP Code) Washington, DC 20305	10 SOURCE OF FUNDING NUMBERS PROGRAM ELEMENT NO: 62715H; PROJECT NO: ; TASK NO: ; WORK UNIT ACCESSION NO: DN580-072

11 TITLE (Include Security Classification)
The Role of Finite Parallel Length on the Stability of Barium Clouds

12 PERSONAL AUTHOR(S)
Sperling, J.L.,* Drake, J.F.,† Zalesak, S.T., and Huba, J.D.

13a TYPE OF REPORT	13b TIME COVERED	14 DATE OF REPORT (Year, Month, Day)	15 PAGE COUNT
Interim	FROM 10/83 TO 10/84	1984 November 8	44

16 SUPPLEMENTARY NOTATION
*JAYCOR, Inc., San Diego, CA 92138 †Science Applications, Inc., McLean, VA 22102 (Continues)

17 COSATI CODES			18 SUBJECT TERMS (Continue on reverse if necessary and identify by block number)
FIELD	GROUP	SUB-GROUP	Barium clouds; Gradient drift instability; Ionospheric structure

19 ABSTRACT (Continue on reverse if necessary and identify by block number)

A simple model is used to show that the finite parallel length of ionospheric plasma clouds can affect the growth rate of striation instabilities (e.g., gradient drift). The finite parallel length of plasma clouds tends to favor the growth of striations with short perpendicular wavelengths.

20 DISTRIBUTION / AVAILABILITY OF ABSTRACT ☒ UNCLASSIFIED/UNLIMITED ☐ SAME AS RPT ☐ DTIC USERS	21 ABSTRACT SECURITY CLASSIFICATION UNCLASSIFIED
22a NAME OF RESPONSIBLE INDIVIDUAL J. D. Huba	22b TELEPHONE (Include Area Code) (202) 767-3630; 22c OFFICE SYMBOL Code 4780

DD FORM 1473, 84 MAR 83 APR edition may be used until exhausted. All other editions are obsolete

SECURITY CLASSIFICATION OF THIS PAGE

16. SUPPLEMENTARY NOTATION (Continued)

This research was sponsored by the Defense Nuclear Agency under Subtask S99QMXBC, work unit 00102 and work unit title "Plasma Structure Evolution."

CONTENTS

THE ROLE OF FINITE PARALLEL LENGTH ON THE STABILITY OF BARIUM CLOUDS

I. INTRODUCTION

In the disturbed ionosphere, Rayleigh-Taylor [Scannapieco and Ossakow, 1976; Ott, 1978; Ossakow et al., 1979; Zalesak and Ossakow, 1980] and gradient drift instabilities [Simon, 1963; Linson and Workman, 1970; McDonald et al., 1980, 1981] are considered to be primary sources for fluid structuring. These instabilities are predicted to be aligned along magnetic field lines with the result that analysis and numerical simulation has emphasized the flute approximation, which neglects the explicit dependence of modes on the coordinate parallel to the ambient magnetic field; when considered, it has been taken into account, in a gross sense, by averaging plasma parameters over magnetic field lines, but without considering the implications on the ionosphere of accompanying mode variation along magnetic field lines. One exception to this generality is the paper by Goldman et al. [1976], which calculates eigenmodes in the electrostatic approximation, recognizing that modes must vary along the magnetic field lines as one moves away from the source of instability, an artificial plasma cloud.

Artificial plasma clouds in the ionosphere have a finite spatial extent that can influence the development and properties of plasma instabilities. In this paper, particular emphasis is placed on determining certain effects on the gradient drift instability resulting from the finite length of plasma clouds along the geomagnetic field. It is demonstrated, with a rather simple plasma geometry, that finite plasma length implies parallel currents and electric fields which contribute to the development of eigenmode structure along the geomagnetic field. Specifically, the finite field-line integrated electron density of ionospheric plasma clouds can play a role in reducing the growth rate of striation instabilities.

Manuscript approved June 27, 1984.

This point is subsequently quantified. The finite parallel length of ionospheric plasma clouds tends to favor the growth of striations with short perpendicular wavelengths.

In Section II, the calculation model and general equations are discussed. Section III contains a derivative of the dispersion equation. Section IV describes the quantitative evaluation of the model for parameters appropriate to barium releases. Concluding remarks are given in Section V.

II. GENERAL EQUATIONS

We first derive a set of nonlinear equations to describe the evolution of a cold plasma cloud ($T = 0$) in a uniform magnetic field $\underset{\sim}{B} = B_0 \hat{z}$ with a background neutral wind $\underset{\sim}{V}_n = V_n \hat{x}$ [see Fig. 1a]. For simplicity we consider only low frequency $\partial/\partial t \ll \nu_\alpha$ motion of the cloud and take the electron collisions to be sufficiently weak so that $\nu_e/\Omega_e \ll 1$ but allow ν_i/Ω_i to be arbitrary. The collision frequency and gyrofrequency of the α species are given by ν_α and Ω_α, respectively. In this limit the fundamental equations of our analysis are continuity, momentum transfer, charge neutrality and Ampere's law:

$$\frac{\partial n_\alpha}{\partial t} + \nabla \cdot (n \underset{\sim}{v}_\alpha) = 0 \qquad (1)$$

$$0 = - e\underset{\sim}{E} - \frac{e}{c} \underset{\sim}{v}_e \times \underset{\sim}{B} - m_e \nu_{en} (\underset{\sim}{v}_e - \underset{\sim}{V}_n) - m_e \nu_{ei} (\underset{\sim}{v}_e - \underset{\sim}{v}_i) \qquad (2)$$

$$0 = e\underset{\sim}{E} + \frac{e}{c} \underset{\sim}{v}_i \times \underset{\sim}{B} - m_i \nu_{in} (\underset{\sim}{v}_i - \underset{\sim}{V}_n) - m_i \nu_{ie} (\underset{\sim}{v}_i - \underset{\sim}{v}_e) \qquad (3)$$

$$\nabla \cdot \underset{\sim}{J} = \nabla \cdot [n_e (\underset{\sim}{v}_i - \underset{\sim}{v}_e)] = 0 \qquad (4)$$

$$\nabla \times \underset{\sim}{B} = \frac{4\pi}{c} \underset{\sim}{J} \tag{5}$$

where the variables have their usual meaning. We take the electric and magnetic fields to be represented by potentials as

$$\underset{\sim}{E} = - \nabla\phi - \frac{1}{c} \frac{\partial A_z}{\partial t} \hat{z} \tag{6}$$

and

$$\underset{\sim}{B} = B_0 \hat{z} + \nabla A_z \times \hat{z} \tag{7}$$

where ϕ is the electrostatic potential and A_z is the vector potential associated with the magnetic field produced by the self-consistent plasma currents. We consider only A_z since $J_\parallel >> J_\perp$ and we assume $|\nabla A_z \times \hat{z}| << B_0$.

The electron cross-field motion is given by

$$\underset{\sim}{v}_{e\perp} = - \frac{c}{B} \nabla_\perp \phi \times \hat{z} \tag{8}$$

while the parallel motion is given by

$$v_{e\parallel} = \frac{e}{m_e \nu_e} [(\hat{b} \cdot \nabla)\phi + \frac{1}{c} \frac{\partial A_z}{\partial t}] \tag{9}$$

where $\nu_e = \nu_{ei} + \nu_{en}$ and $\hat{b} = \underset{\sim}{B}/B_0$.

The ion cross-field motion is given by

$$\underset{\sim}{v}_{i\perp} = \delta\left[-\frac{c}{B}\nabla_\perp\phi \times \hat{z} + \frac{\nu_{in}}{\Omega_i}\underset{\sim}{V}_n \times \hat{z}\right.$$

$$\left.-\frac{\nu_{in}}{\Omega_i}\frac{c}{B}\nabla_\perp\phi + \left(\frac{\nu_{in}}{\Omega_i}\right)^2\underset{\sim}{V}_n\right], \qquad (10)$$

where $\delta = \left(1 + \nu_{in}^2/\Omega_i^2\right)^{-1}$, and the parallel motion is given by

$$v_{i\parallel} = -\frac{e}{m_i\nu_{in}}\frac{\nu_{en}}{\nu_e}\left[(\hat{b}\cdot\nabla)\phi + \frac{1}{c}\frac{\partial A_z}{\partial t}\right] \qquad (11)$$

In (10) we have included both the Pedersen and Hall responses to the electric field and neutral wind, while in (11) we have assumed $m_e\nu_{en} << m_i\nu_{in}$.

Substituting (8)-(11) into (1), (4) and (5) we find that

$$\frac{dn}{dt} - \frac{c}{B}\nabla\hat{\phi} \times \hat{z}\cdot\nabla n + \frac{c}{4\pi e}(\hat{b}\cdot\nabla)\nabla_\perp^2 A_z = 0 \qquad (12)$$

$$\delta\frac{\nu_{in}^2}{\Omega_i^2}\frac{c}{B}\nabla n\cdot\nabla_\perp\hat{\phi} \times \hat{e}_z - \delta\frac{\nu_{in}}{\Omega_i}\frac{c}{B}\nabla\cdot n\nabla_\perp\hat{\phi} + \frac{\nu_{in}}{\Omega_i}\nabla n\cdot\underset{\sim}{V}_n \times \hat{e}_z$$

$$-\frac{c}{4\pi e}(\hat{b}\cdot\nabla)\nabla_\perp^2 A_z = 0 \qquad (13)$$

$$\nabla_\perp^2 A_z = \frac{4\pi}{c\eta_e}\left[(\hat{b}\cdot\nabla)\hat{\phi} + \frac{1}{c}\frac{dA_z}{dt}\right] \qquad (14)$$

where $\hat{\phi} = \phi - (B/c)(\nu_{in}/\Omega_i)\underset{\sim}{V}_n\cdot\underset{\sim}{x}$, $d/dt = \partial/\partial t + (\nu_{in}/\Omega_i)\hat{z} \times \underset{\sim}{V}_n\cdot\nabla$, and $\eta_e = m_e\nu_e/ne^2$. Equation (12) is the electron continuity equation, (13) is the charge conservation equation, and (14) is Ampere's law. Thus, (12)-(14) provide a complete description of the evolution of a three-dimensional, cold plasma cloud.

We will only consider the linear stability of a two-dimensional cloud which is localized both along and across the magnetic field B_0: $n_c = n_c(x,z)$ with $|x| \lesssim x_0$ and $|z| \lesssim z_0$. The background plasma is taken to be uniform throughout all space. The equations describing this two-dimensional equilibrium are given by

$$\frac{\partial n}{\partial t} + \frac{1}{e}\frac{\partial}{\partial z}\frac{1}{n_e}\left(\frac{1}{c}\frac{\partial A_z}{\partial t} + \frac{\partial \hat{\phi}}{\partial z}\right) = 0 \qquad (15)$$

$$\delta \frac{\nu_{in}}{\Omega_i}\frac{c}{B}\frac{\partial}{\partial x} n \frac{\partial \hat{\phi}}{\partial x} + \frac{c}{4\pi e}\frac{\partial}{\partial z}\frac{\partial^2 A_z}{\partial x^2} = 0 \qquad (16)$$

$$\frac{\partial^2 A_z}{\partial x^2} = \frac{4\pi}{cn_e}\left(\frac{1}{c}\frac{\partial A_z}{\partial t} + \frac{\partial \hat{\phi}}{\partial z}\right) \qquad (17)$$

From (15)-(17) we find that the equilibrium is given by $A_z = \hat{\phi} = 0$ with $n_c(x,z)$ an arbitrary function. For simplicity we consider the plasma density to be given by [similar to that used by Sperling (1983a)]

$$n(x,z) = \begin{array}{ll} n_< = n_c(x) + n_b & |z| < z_0 \\ n_> = n_b & |z| > z_0 \end{array} . \qquad (18)$$

where the subscripts c and b refer to cloud and background, respectively, [see Fig. 1b].

We note that if we had retained a finite plasma temperature then the density equation would be

$$\frac{\partial n}{\partial t} - \frac{\partial}{\partial z}\frac{T}{m_i \nu_{in}}\frac{\partial n}{\partial z} = 0 \qquad (19)$$

where $T = T_e + T_i$ and we have taken $\partial/\partial x = 0$. Equation (19) describes the diffusion of the cloud along z with a diffusion coefficient, $D_z = T/m_i \nu_{in}$. Thus, in general (15)-(17) will not have equilibrium solutions when $\partial/\partial z \neq 0$ and $T \neq 0$. However, in calculating the growth rates of unstable modes with growth times which are short compared with the diffusion time $t_z = z_0^2/D_z$, we would expect the evolution of the equilibrium to have very little influence on the stability calculation for this situation. Consideration of finite temperature effects will be deferred to a later report.

III. LINEARIZED EQUATIONS AND DISPERSION RELATION

To find the influence of the parallel dynamics on the instability, we linearize (7)-(9) where the perturbed quantities vary as $\tilde{p} \sim \tilde{p}(z) \exp\left(\gamma t + ik_y y\right)$. After eliminating the equation for $\tilde{n}$ algebraically, we obtain two coupled differential equations for $\tilde{A}_z$ and $\tilde{\phi}$,

$$\left(\bar{\gamma} + k_y^2 D_r\right)\tilde{A}_z = - c \frac{\partial \tilde{\phi}}{\partial z} \tag{20}$$

$$\left(\bar{\gamma} - \gamma_0\right)\tilde{\phi} = - \gamma \alpha D_r \frac{1}{c} \frac{\partial \tilde{A}_z}{\partial z} \tag{21}$$

where $\gamma_0 = - n_<' V_n/n_< \delta$, $n_<' = \partial n_</\partial x$, $\bar{\gamma} = \gamma + ik_y V_n \nu_{in}/\Omega_i$, $D_r = \nu_e c^2/\omega_{pe}^2$ is the resistive diffusion coefficient, and $\alpha = \Omega_e \Omega_i/\nu_e \nu_{in} \delta$.

Prior to solving (20) and (21) for the density profile given by (18), we first consider a cloud of infinite extent $\left[z_0 \to \infty \text{ in } (18)\right]$ and Fourier expand modes parallel to B_0, i.e., $\tilde{p}(z) \sim \tilde{p} \exp\left(ik_z z\right)$. We consider the local approximation $\left[k_y (n'/n)^{-1} >> 1\right]$ so that (20) and (21) can be solved algebraically. This allows comparison with previous results [Sperling, 1983b; Basu and Coppi, 1983] and insight into the effects of finite parallel wavelengths. The local dispersion equation is given by

$$(\bar{\gamma} - \gamma_0)(\bar{\gamma} + k_y^2 D_r) = - \gamma \alpha k_z^2 D_r \tag{22}$$

We note that the RHS of (22) can be expressed as $- \gamma k_z^2 V_A^2/\nu_{in}\delta_i$ where $V_A = B/(4\pi n m_i)^{1/2}$ is the Alfvén velocity. This form explicitly shows the coupling to an Alfvén wave which is the dominant finite k_z effect. For simplicity we assume $\gamma >> k_y V_n(\nu_{in}/\Omega_i)$ and solve (22) in two limits: $\gamma >> k_y^2 D_r$ (electromagnetic limit) and $\gamma << k_y^2 D_r$ (electrostatic limit). It is found that

$$\hat{\gamma} = 1 - \hat{k}_z^2 = 1 - k_z^2 V_A^2/\gamma_0 \nu_{in}\delta_i \qquad (\gamma >> k_y^2 D_r) \tag{23}$$

and

$$\gamma = (1 + \hat{k}_z^2/\hat{k}_y^2)^{-1} \qquad (\gamma << k_y^2 D_r) \tag{24}$$

where $\hat{\gamma} = \gamma/\gamma_0$, $\hat{k}_y = k_y L_r$, $\hat{k}_z = k_z z_r$, and L_r and z_r are the perpendicular and parallel resistive length scales given by $L_r^2 = D_r/\gamma_0$ and $z_r^2 = \alpha D_r/\gamma_0$. In the ideal limit ($D_r = 0$), (23) indicates that electromagnetic effects stabilize the instability when $\hat{k}_z^2 > 1$ (i.e., $k_z^2 V_A^2 > \gamma_0 \nu_{in}\delta_i$) by coupling to an Alfvén wave. This result is similar to that of Basu and Coppi [1983] who investigated the collisional Rayleigh-Taylor instability. On the other hand, (24) indicates that in the electrostatic limit there is only a reduction in growth rate. This is because resistive diffusion across the magnetic field lines is sufficiently rapid to dissipate the Alfvén wave. Finally, in the limit $k_z \to 0$ we recover from (22) the standard result $\gamma = \gamma_0 - ik_yV_n(\nu_{in}/\Omega_i)$, where the real frequency is caused by the equilibrium electric field in the x direction; in a frame of reference moving with the electrons, however, the mode has no real frequency. A second mode, which is damped is given by $\gamma = -k_y^2D_r - ik_yV_n(\nu_{in}/\Omega_i)$ [Chu et al., 1978; Sperling, 1983b].

For a general profile n(x,z) the coupled equations for $\tilde{\phi}$ and $\tilde{A}_z$ must be solved subject to the boundary conditions $\tilde{\phi}$, $\tilde{A}_z \to 0$ as $|z| \to \infty$. For the step profile for n(x,z) given in (15), the solutions to (20) and (21) in the region $|z| > z_0$ can be written as plane waves,

$$\tilde{A}_z = \tilde{A}_{z>} \exp[-k_>|z|], \tag{25a}$$

$$\tilde{\phi} = \hat{\phi}_> \exp[-k_>|z|], \tag{25b}$$

with

$$(\bar{\gamma}_> + k_y^2D_{r>})\tilde{A}_{z>} = k_>c\,\tilde{\phi}_>, \tag{25c}$$

$$\frac{k_>^2}{k_y^2} = \left(\frac{\bar{\gamma}}{\gamma}\frac{1}{\alpha R}\right)_> \tag{25d}$$

where

$$R = \frac{k_y^2D_r}{\gamma + k_y^2D_r} \tag{25e}$$

and the subscript > on a given parameter indicates that it is to be evaluated in the region $|z| > z_0$. Note that the solutions which diverge as $z \to \pm \infty$ have been omitted in (25a) and (25b). The parameter R is a measure of the electrostatic or electromagnetic nature of the mode. For $k_y^2 D_r >> \gamma$, we note that $R \sim 1$ and the mode is essentially electrostatic. In the opposite limit $k_y^2 D_r << \gamma$, the mode is electromagnetic and $R << 1$.

In the region $|z| < z_0$, the solutions for $\tilde{\phi}$ and $\tilde{A}_z$ are

$$\tilde{A}_z = \tilde{A}_{z<}^1 \sin(k_< z) - \tilde{A}_{z<}^2 \cos(k_< z) \tag{26a}$$

$$\tilde{\phi} = \tilde{\phi}_<^1 \cos(k_< z) + \tilde{\phi}_<^2 \sin(k_< z) \tag{26b}$$

with

$$(\bar{\gamma}_< + k_y^2 D_{r<})\tilde{A}_{z<}^{1,2} = k_< c\, \tilde{\phi}_<^{1,2} \tag{26c}$$

$$\frac{k_<^2}{k_y^2} = \left(\frac{\gamma_0 - \bar{\gamma}}{\gamma} \frac{1}{\alpha R}\right)_< \tag{26d}$$

To complete the dispersion relation, we must match the various plane wave solutions at $z = \pm z_0$. The appropriate matching conditions are obtained from (20) and (21). Integrating these two equations across the discontinuity in the density at $z = \pm z_0$, we find that $\tilde{\phi}$ and $\tilde{A}_z$ must be continuous. For the even $\tilde{\phi}$ solution ($\tilde{\phi}_<^2 = 0$), we obtain the dispersion relation for the growth rate γ,

$$k_< z_0 = \tan^{-1}\left[\frac{k_>}{k_<} \frac{\bar{\gamma} + k_y^2 D_{r<}}{\bar{\gamma} + k_y^2 D_{r>}}\right] + m\pi \tag{27}$$

where m is an integer. The dispersion relation for the odd $\tilde{\phi}$ mode $(\tilde{\phi}_{<}^{1} = 0)$ is similar to (27) except $\tan^{-1}$ is replaced by $-\cot^{-1}$.

In general, the dispersion equation (27) has an infinite number of solutions for a given set of physical parameters, corresponding to eigenmodes with an increasing number of modes (m) along z. The dispersion equation (27) can be solved numerically for arbitrary values of the background and cloud parameters. However, to gain an understanding of the general scaling of the growth rate γ with the parallel extent of the cloud, it is useful to solve (27) analytically. To do this we make a number of simplifying assumptions. We consider only the lowest order mode (i.e., m = 0 which implies $0 < k_{<}z_0 < \pi/2$; it is easily shown that this mode has the largest growth rate); take ν_{in}/Ω_i to be small so that $\delta \simeq 1$ and the real frequency, $k_y V_n \nu_{in}/\Omega_i$, can be neglected; and finally, take all parameters but the density to be the same inside and outside of the cloud. In this limit the expressions for $k_{\gtrless}$ reduce to

$$\frac{k_{>}^{2}}{k_y^{2}} = (\alpha R)_{>}^{-1} \tag{28a}$$

$$\frac{k_{<}^{2}}{k_y^{2}} = \frac{\gamma_0 - \gamma}{\gamma} \, (\alpha R)_{<}^{-1} \tag{28b}$$

We separate our analysis into two separate cases $\nu_{ei} \gtrless \nu_{en}$. In the limit $\nu_{ei} \gg \nu_{en}$, the resistive diffusion coefficient D_r is continuous across the cloud boundary and $R_{>} = R_{<}$.

With these assumptions the dispersion equation (27) becomes

$$k_< z_0 = \tan^{-1}\left[\left(\frac{\hat{\gamma}}{1-\hat{\gamma}}\frac{n_>}{n_<}\right)^{1/2}\right] \tag{29a}$$

with

$$k_<^2 z_0^2 = [(1-\hat{\gamma})/\hat{\gamma}](n_</n_>)(\hat{\gamma} + \hat{k}_y^{\,2})\hat{z}_0^{\,2}, \tag{29b}$$

and $\hat{z}_0 = z_0/z_r$, $\hat{k}_y = k_y L_r$ where $L_r^2 = D_{r>}/\gamma_o$ and $z_r^2 = \alpha_> L_r^2$. The dispersion relation in (29) is now a function of only three parameters: $\hat{z}_0$, $n_>/n_<$ and $\hat{k}_y$.

In the limit

$$[(1-\hat{\gamma})/\hat{\gamma}](n_</n_>) \ll 1, \tag{30}$$

the arctan function approaches $\pi/2$ so that $k_< z_0 \simeq \pi/2$ is the dispersion equation. Furthermore, since $n_</n_> = (n_c + n_b)/n_b > 1$, the inequality in (30) can only be satisfied for $\hat{\gamma} \simeq 1$. Thus, the growth rate is given by

$$\hat{\gamma} \simeq 1 - \frac{\pi^2}{4\hat{z}_0^2}\frac{n_>}{n_<} \qquad \text{for} \qquad \hat{\gamma} \gg \hat{k}_y^2 \tag{31a}$$

and

$$\hat{\gamma} \simeq \left(1 + \frac{\pi^2}{4\hat{z}_0^2}\frac{n_>}{n_<}\frac{1}{\hat{k}_y^2}\right)^{-1} \qquad \text{for} \qquad \hat{\gamma} \ll \hat{k}_y^2 \tag{31b}$$

We note that (31a) and (31b) can be compared to the local growth rates (23) and (24) if we define an effective $\hat{k}_{zeff}$

$$\hat{k}^2_{zeff} \equiv \frac{\pi^2}{4\hat{z}_0^2} \frac{n_>}{n_<} . \tag{32}$$

Thus, taking $\hat{k}^2_z = \hat{k}^2_{zeff}$ in (23) and (24) we recover (31a) and (31b). For $m \neq 0$ modes, $\hat{k}_{zeff}$ becomes $(m + 1/2)^2\pi^2/4\hat{z}_0^2(n_>/n_<)$ indicating a spectrum of modes parallel to $\underset{\sim}{B}$. Finally, since $\hat{\gamma} \sim 1$ from (31a) and (31b) we can write a generalized dispersion relation given by

$$\hat{\gamma} = 1 - \frac{\pi^2}{4\hat{z}_0^2} (1 + \hat{k}_y^2)^{-1} \frac{n_>}{n_<} \tag{33a}$$

and is valid for [based on (30)]

$$(1 + \hat{k}_y^2)\hat{z}_0^2 >> 1. \tag{33b}$$

In the opposite limit, i.e.,

$$[(1 - \hat{\gamma})/\hat{\gamma}](n_</n_>) >> 1, \tag{34}$$

arctan function approaches $k_< z_0$. The dispersion relation becomes

$$(1 - \hat{\gamma})(\hat{\gamma} + \hat{k}_y{}^2)^{1/2} = \hat{\gamma}\, n_>/n_< \hat{z}_0 . \tag{35}$$

The solution of the equation is

$$\hat{\gamma} = 1 - (n_>/n_<)\hat{z}_0^{-1}(1 + \hat{k}_y{}^2)^{-1/2} \simeq 1 \tag{36a}$$

for

$$(n_>/n_<)^2 \ll (1 + \hat{k}_y^{\,2})\hat{z}_0^{\,2} \ll 1, \qquad (36b)$$

where the inequalities follow from (34) and the condition $\hat{\gamma} \simeq 1$. When $\hat{\gamma} \ll 1$, (35) becomes a quadratic equation with the solution

$$\hat{\gamma} = \hat{z}_0^{\,2}(n_</n_>)^2[1 + (1 + 4\,\hat{k}_y^{\,2}\hat{z}_0^{-2}n_>^2/n_<^2)^{1/2}]/2, \qquad (37a)$$

which is valid for (from $\hat{\gamma} \ll 1$)

$$(1 + \hat{k}_y^{\,2})\hat{z}_0^{\,2} \ll n_>^2/n_<^2 \,. \qquad (37b)$$

For $\hat{z}_0$ very small the growth rate approaches zero as

$$\hat{\gamma} \simeq \hat{k}_y\hat{z}_0 n_</n_>. \qquad (38)$$

Equation (38) also implies that the growth rate increases with $\hat{k}_y$ in this region. The physical reason for this behavior will be discussed shortly.

The growth rates and inequalities in (33), (36) and (37) can be summarized rather succinctly in the $(n_>/n_<) - \hat{z}_0$ phase space plot shown in Fig. 2. Note that $n_>/n_< = n_b/(n_b + n_c) < 1$. Regions I, II and III indicate the range of validity of the growth rates in (33), (36) and (37), respectively. Expressions for the growth rate in these three regions are given in Table I. For large $\hat{z}_0$, in Regions I and II, the finite length of the cloud along $\underset{\sim}{B}$ has very little influence on the growth rate and $\hat{\gamma} \sim \gamma/\gamma_0 \sim 1$. For small $\hat{z}_0$, in Region III, $\hat{\gamma} \ll 1$ so that the finite extent of the cloud strongly reduces the growth rate. As $\hat{k}_y$ increases, Region III shrinks in size so that the growth rates for short wavelength modes are less affected by the parallel dynamics than are the growth rates for long wavelength modes. Nevertheless, (25d) shows that the short wavelength modes are more localized along the magnetic field than long wavelength modes [Sperling and Glassman, 1983; Sperling, 1984].

In Fig. 3 we schematically show the growth rate $\hat{\gamma}$ as a function of $\hat{z}_0$ for $n_>/n_<$ and $\hat{k}_y \ll 1$ held fixed. In Region III the growth rate first increases linearly with $\hat{z}_0$ and then quadratically until $\hat{\gamma} \sim 1$, where it enters Regions II. The transition from $\hat{\gamma} \sim \hat{z}_0$ to $\hat{\gamma} \sim \hat{z}_0^{\,2}$ in Region III is a consequence of the change in character of the mode from being dominantly electrostatic $(\gamma < k_y^2 D_r)$ for $\hat{z}_0 < \hat{k}_y n_>/n_<$ to electromagnetic $(\gamma > k_y^2 D_r)$ for $\hat{z}_0 > \hat{k}_y n_>/n_<$.

The dependence of the growth rate on $\hat{k}_y$ can also be readily obtained from Fig. 2 and Table I. For parameters $\hat{z}_0$ and $n_>/n_<$ such that modes with $\hat{k}_y \ll 1$ are in Regions I and II $(\hat{z}_0 > n_>/n_<)$, $\hat{\gamma} \sim 1$ for all $\hat{k}_y$ since increasing $\hat{k}_y$ simply pushes the mode further into Regions I and II. For the case where modes with $\hat{k}_y \ll 1$ fall in Region III $(\hat{z}_0 < n_>/n_<)$, the dependence of $\hat{\gamma}$ on $\hat{k}_y$ is more interesting. In Fig. 4 the growth rate is shown versus $\hat{k}_y$ with $n_>/n_<$ and $\hat{z}_0$ held fixed. For small $\hat{k}_y$ the mode falls in Region III and has a growth rate nearly independent of $\hat{k}_y$. When $\hat{k}_y > \hat{z}_0 n_</n_>$, the mode becomes electrostatic and the growth rate increases with $\hat{k}_y$ until $\hat{k}_y \sim n_>/n_< \hat{z}_0$ when $\hat{\gamma} \sim 1$ and the mode enters Region II. We again conclude from this figure that the growth rates for short wavelength modes are less affected by the parallel dynamics than the growth rates for long wavelength modes.

Up to this point we have discussed only the case where $\nu_{ei} \gg \nu_{en}$. The dispersion equation (27) can be solved in a similar manner in the opposite limit $\nu_{ei} \ll \nu_{en}$. In this limit the resistive diffusion coefficient is not continuous across the cloud boundaries at $\pm z_0$. The results differ only slightly from those just presented so we skip the details and simply present the analogues of Fig. 2 and Table I for this case. In Fig. 5 we show the $(n_>/n_<) - \hat{z}_0$ phase space plot showing the three regions of the instability for $\nu_{en} \gg \nu_{ei}$. The growth rates for these three regions are listed in Table II. The only difference between phase space plots in Figs. 2 and 5 is the boundary between Regions I and II, which falls at larger $\hat{z}_0$ when $\nu_{en} \gg \nu_{ei}$. The growth rates for $\nu_{en} \gtrless \nu_{ei}$ differ only in Region I. Since $\hat{\gamma} \sim 1$ in both Regions I and II, these differences are not particularly significant so the previous discussion of the instability in the limit $\nu_{ei} \gg \nu_{en}$ also applies to the opposite limit.

We have shown that the finite length z_0 of the plasma cloud reduces the growth rate of the gradient drift instability compared with its value when z_0 is infinite. The growth rates of long wavelength modes are more strongly reduced than those of short wavelength modes. The essential physics which underlies these results can be understood by integrating (21) for the perturbed potential $\tilde{\phi}$ along z,

$$\gamma \int_{-\infty}^{\infty} dz\ n(z)\tilde{\phi}(z) = \gamma_0 \int_{-z_0}^{z_0} dz\ n(z)\tilde{\phi}(z) \simeq 2\gamma_0 n_< z_0 \tilde{\phi}_<, \qquad (39)$$

where we have again taken ν_{in}/Ω_i small and we have assumed that $\tilde{\phi}(z) \simeq$ const in the region $|z| < z_0$, which is approximately correct for the lowest order mode. The integral on the left side of (39) represents the integrated Pederson conductivity along the entire field line, weighted by the potential $\tilde{\phi}$. The integral on the right side of this equation is the integrated Pederson conductivity of the cloud. Carrying out the remaining integral, we find

$$\gamma \simeq \gamma_0 n_< z_0 \tilde{\phi}_< / (n_< z_0 \tilde{\phi}_< + n_> k_>^{-1} \tilde{\phi}_>)$$

$$\simeq \gamma_0 n_< z_0 / (n_< z_0 + n_> k_>^{-1}), \tag{40}$$

where we have used the results of our previous calculation: $\tilde{\phi}_< \simeq \tilde{\phi}_>$ and $\tilde{\phi} \rightarrow 0$ when $k_> |z| > 1$. Substituting the expression for $k_>$ in (25d) into (40), we obtain the dispersion relation

$$\gamma = \gamma_0 \frac{n_< z_0}{n_< z_0 + n_> k_y^{-1} (\alpha R)_>^{1/2}} . \tag{41}$$

When the result is written in the normalized variables presented previously, it reduces precisely to the dispersion relation presented in (35). The reduction of the growth rates due to finite z_0 occur because the integrated Pederson conductivity over the extent of the mode along z becomes comparable to that of the cloud. The distance the mode extends along z $(\sim k_>^{-1})$ increases as k_y decreases [see (25d)] so that long wavelength modes have greater reductions in their growth rates. The electromagnetic effects prevent the mode from extending an infinite distance along the magnetic field line as $k_y \to 0$. In this limit $R_> \to 0$ and (41) becomes

$$\gamma = \gamma_0 \frac{n_< z_0}{n_< z_0 + n_> \left(\frac{\alpha D_r}{\gamma}\right)_>} \tag{42}$$

so that the growth rate is independent of k_y as shown in Fig. 4.

IV. RESULTS

The plasma model outlined in Sections II and III is rather simple, and admittedly does not include all the intricacies and inhomogeneities of the real ionosphere. Nevertheless, the model does show that the growth rate is a function of the parallel length. We now present quantitative results of our model for typical ionospheric parameters. In particular, we take $n_< = 10^7 cm^{-3}$, $n_> = 10^5 cm^{-3}$, $B = 0.4$ G, $T_i = T_e = 0.1$ eV, and consider two values of γ_0: $\gamma_0 = 0.01\ sec^{-1}$ and $\gamma_0 = 0.10\ sec^{-1}$. The ions for $|z| < z_0$ are assumed to be barium (i.e., $m_{i<} = 137\ m_p$, with m_p the proton mass) and the ions for $|z| > z_0$ are assumed to be air with $m_{i>} = 20\ m_p$. The mass of an atmospheric neutral particle, $m_{0<(>)}$, is also assumed to be 20 m_p. The neutral density, $n_{0<} = n_{0>} = 8.3 \times 10^9\ cm^{-3}$, is appropriate to an altitude of ~ 200 km [Knapp and Schwartz, 1975]. The collision frequencies are determined from [Braginskii, 1965; Kilb, 1977)

$$\nu_{i<} = 2.5 \times 10^{12} m_0 n_0 \tag{42a}$$

$$\nu_{i>} = 2.5 \times 10^{13}\ m_0 n_0 \tag{42b}$$

$$\nu_{e<(>)} = 0.51\ \nu_{ei<(>)} + 1.9 \times 10^{-8}\ n_0 \qquad (42c)$$

$$\nu_{ei<(>)} = 1.1 \times 10^{-3}\ n_{e<(>)}. \qquad (42d)$$

In (42) all parameters are in cgs units. Based upon these parameters and equations we can calculate the perpendicular and parallel resistive scale lengths which are given in Table III for $\gamma_0 = 0.01$ sec^{-1} and 0.1 sec^{-1}.

An important result to be considered is the boundary between Regions II and III in Figs. 2 and 5. The boundary is defined by the equation

$$\frac{n_>}{n_<} = (1 + \hat{k}_y^{\,2})^{1/2}\ \hat{z}_{0c} \qquad (43)$$

and marks the transition between strong and weak growth. For $\hat{z}_0 < \hat{z}_{0c}$ the theory predicts very weak growth, and it is clear that the long wavelength modes ($\hat{k}_y \ll 1$) have the weakest growth for a given value of $\hat{z}_0$ and $n_>/n_<$. In Fig. 6 we plot z_{0c} (km) vs. k_y (km^{-1}) based on (43) for $n_>/n_< = 0.01$ and the parameters described above and in Table III. The regions below each curve indicate weak growth, while regions above each curve indicate strong growth. As expected, the value of z_{0c} is largest for $k_y \ll 1$. Also, we note that the dependence of z_{0c} on k_y is stronger for smaller values of wavenumber ($k_y < 1$ km^{-1}) and γ_0.

In Fig. 7 we plot $\hat{\gamma} = \gamma/\gamma_0$ vs. k_y (km^{-1}) for the parameters given above and different values of z_0. The solid lines are based on $\gamma_0 = 0.10$ sec^{-1} while the dashed lines are for $\gamma_0 = 0.01$ sec^{-1}. These figures are based upon (35). Again, these curves quantitatively reflect the growth rate dependence on k_y and z_0 which is presented qualitatively in Fig. 4. For $k_y > 2$ km^{-1}, the normalized growth rate $\hat{\gamma}$ is independent of z_0. This is consistent with Fig. 6 which shows that $z_{\eta c}$ is independent of γ_η for $k_y > 2\ \mathrm{km}^{-1}$. On the other hand, for $k_y < 2\ \mathrm{km}^{-1}$ the difference between the curves becomes larger, especially for z_η large. Again, this is consistent with Fig. 6 which indicates a strong dependence of $z_{\eta c}$ on γ_η for $k_y < 2\ \mathrm{km}^{-1}$. It is clear from Fig. 7 that the finite parallel extent of the cloud favors the growth of short wavelength modes.

V. CONCLUDING REMARKS

We have presented a linear analysis of the gradient drift instability appropriate to ionospheric plasma clouds of finite spatial extent, both perpendicular and parallel to the ambient magnetic field. Based on a simple model for the cloud [see (18)], we find that the parallel extent of the cloud along $\underset{\sim}{B}$ can significantly alter the growth rate of the instability. Specifically, we find that long wavelength modes (k_y small) tend to have much smaller growth rates than short wavelength modes (k_y large). This reduction in growth due to finite z_η occurs because the integrated Pedersen conductivity of the background plasma over the extent of the mode along z becomes greater than that of the cloud [see (40)]. The distance the mode extends along z increases as k_y decreases [see (25d)] so that the long wavelength modes are more strongly affected. A more detailed numerical analysis of this effect is given in Sperling and Glassman (1983). We mention that these results also apply to the $E \times B$ gradient drift [McDonald et al., 1980, 1981] and Rayleigh-Taylor [Ossakow et al., 1979; Sperling, 1982] instabilities.

A question which naturally arises is, how does the growth rate change as the cloud diffuses along the magnetic field or, more generally, as the cloud evolves in time? It is tempting to conclude that the growth rate simply increases with z_0 as the cloud diffuses along z as shown in Figs. 3 and 6. However, as the cloud diffuses along z we expect the electron density inside the cloud to decrease such that $n_< z_0 \sim$ constant. Loosely speaking, the total number of cloud electrons along a given magnetic field line should not change, or at least, not change significantly. Since the growth rates of the instability in the weak (Region III) and strong (Region II) growth regions depend only on the product $n_< z_0$, parallel diffusion along z does not cause the growth rate to increase. The expansion of the cloud along z also does not enable the mode to change from weak to strong growth. This is clearly seen from (43) which indicates that the boundary between Regions II and III does not change in time as long as $n_< z_0 \sim$ constant. Thus, we conclude that just diffusion of the cloud along z does not change the growth rate in an important way.

On the other hand, the gross evolution of the cloud involves not only diffusion along z but, for example, steepening of the "backside" of the cloud which increases the growth rate γ_0. As shown in Fig. 6, for a given value of z_0 more modes are in the strong growth regime when γ_0 is larger. Thus, the parallel dynamics will significantly change the spectrum of unstable modes as the cloud evolves in time. This feature may be related to the observation of the delayed onset of striations. That is, the onset of striations in barium clouds occurs several minutes after the detonation of the barium release. Specifically for larger barium clouds, like Spruce [Linson and Meltz, 1972], the onset time for striations is estimated to be generally greater than approximately 5 minutes [McDonald et al., 1980]. Linson and Meltz (1972) have estimated that the Spruce and Olive ion clouds had an extent approximately 30-40 km extent along the magnetic field at about 5 minutes. This parallel extent corresponds to $z_0 \approx$ 15-20 km. It is possible then that plasma clouds need to evolve in time so that they have a sufficiently steepened "backside", as well as a sufficient length along $\underset{\sim}{B}$, before the striations can occur rapidly.

ACKNOWLEDGMENT

This work was supported by the Defense Nuclear Agency.

TABLE I: GROWTH RATES ($\nu_{ei} \gg \nu_{en}$)

Region	Growth Rate
I	$\hat{\gamma} = 1 - \left(\frac{\pi^2}{4}\right) \frac{1}{\hat{z}_0^2} \frac{1}{(1 + \hat{k}_y^2)} \frac{n_>}{n_<} \approx 1$
II	$\hat{\gamma} = 1 - \frac{1}{\hat{z}_0} \frac{1}{(1 + \hat{k}_y^2)^{1/2}} \frac{n_>}{n_<} \approx 1$
III	$\hat{\gamma} = \hat{z}_0^2 \left(\frac{n_<}{n_>}\right)^2 \left[1 + \left(1 + \frac{4\hat{k}_y^2}{\hat{z}_0^2} \frac{n_>^2}{n_<^2}\right)^{1/2}\right] \ll 1$

TABLE II: GROWTH RATES ($\nu_{ei} \ll \nu_{en}$)

Region	Growth Rate
I	$\hat{\gamma} = 1 - \frac{\pi^2}{4} \frac{1}{\hat{z}_0^2} \frac{1}{\left[1 + \hat{k}_y^2(n_>/n_<)\right]} \frac{n_>}{n_<} \approx 1$
II	$\hat{\gamma} = 1 - \frac{1}{\hat{z}_0} \frac{1}{(1 + \hat{k}_y^2)^{1/2}} \frac{n_>}{n_<} \approx 1$
III	$\hat{\gamma} = \hat{z}_0^2 \left(\frac{n_<}{n_>}\right)^2 \left[1 + \left(1 + \frac{4\hat{k}_y^2}{\hat{z}_0^2} \frac{n_>^2}{n_<^2}\right)^{1/2}\right] \ll 1$

TABLE III: RESISTIVE SCALE LENGTHS

		$\gamma_0 = 0.01\ \mathrm{sec}^{-1}$	$\gamma_0 = 0.10\ \mathrm{sec}^{-1}$
Perpendicular:	L_r	2.5 km	0.8 km
Parallel:	z_r	2370 km	750 km

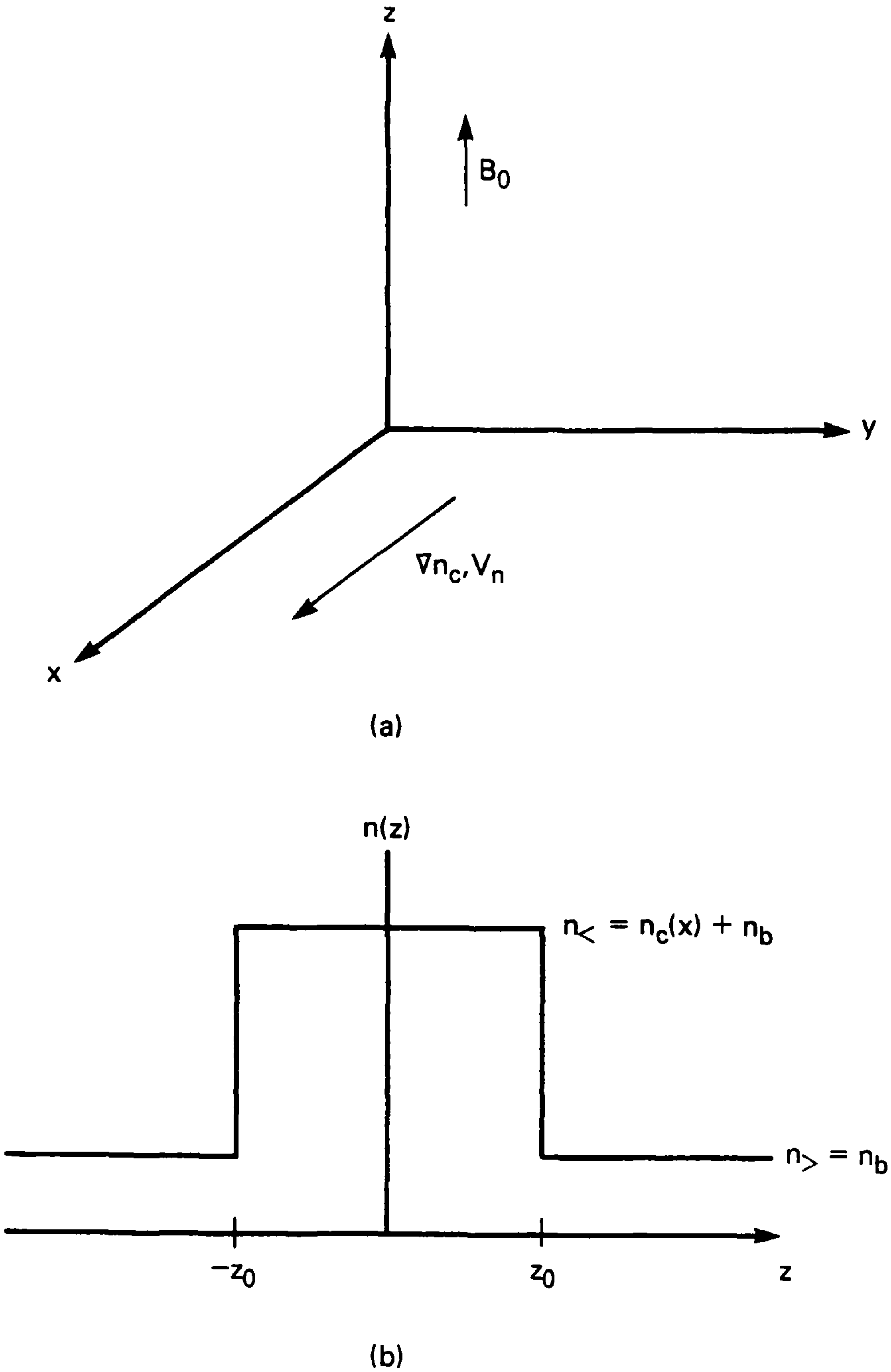

Fig. 1 Plasma configuration and geometry. (a) Coordinate system. (b) Density profile parallel to $\underset{\sim}{B}_0$.

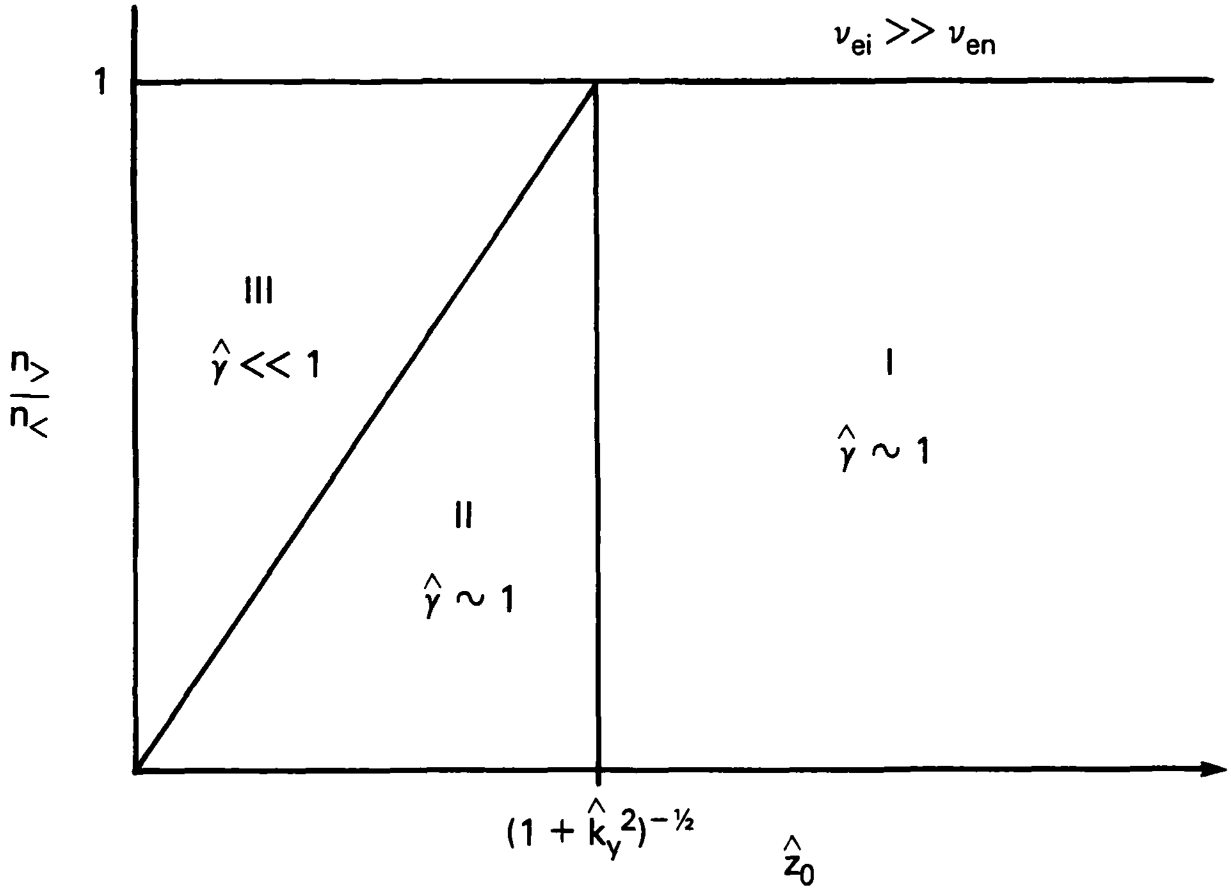

Fig. 2 Regions of validity for the growth rates given by (33), (36), and (37). The growth rates are listed in Table I and are based upon the assumption that $\nu_{ei} >> \nu_{en}$.

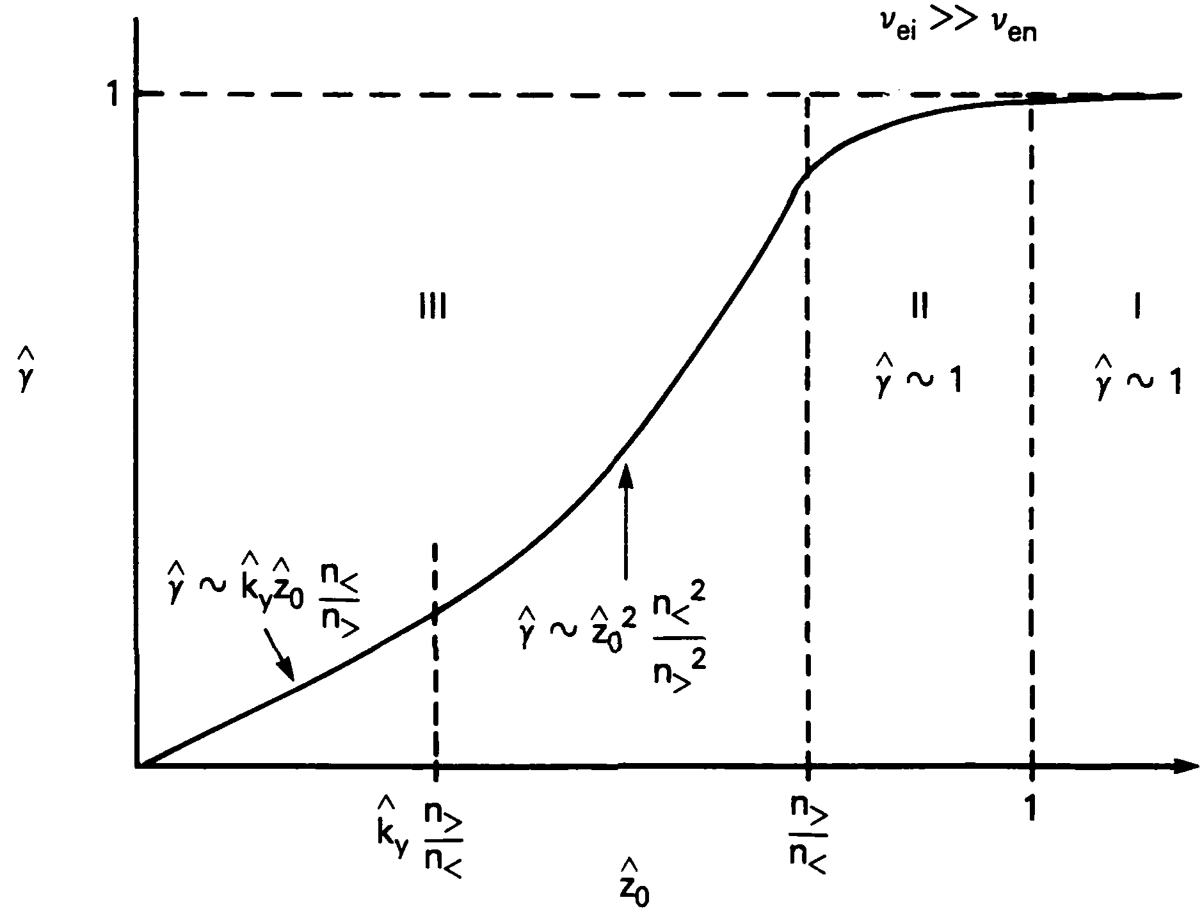

Fig. 3 Schematic of the growth rate $\hat{\gamma}$ vs. parallel length $\hat{z}_0$ for fixed $n_>/n_<$ and $\hat{k}_y$. This curve is based on the assumption that $\nu_{ei} >> \nu_{en}$.

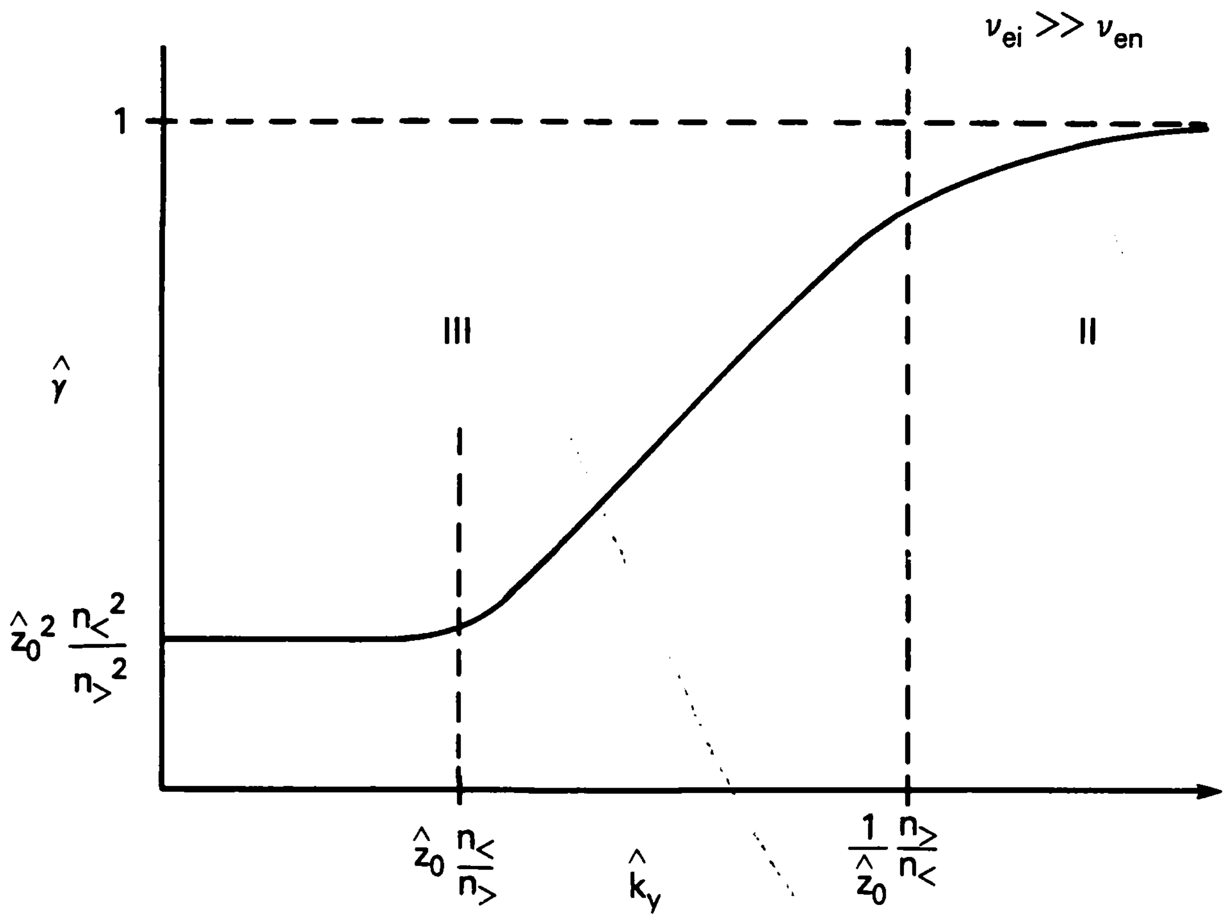

Fig. 4 Schematic of the growth rate $\hat{\gamma}$ vs. perpendicular wavenumber $\hat{k}_y$ for fixed $n_>/n_<$ and $\hat{z}_0$. This curve is based upon the assumption that $\nu_{ei} >> \nu_{en}$.

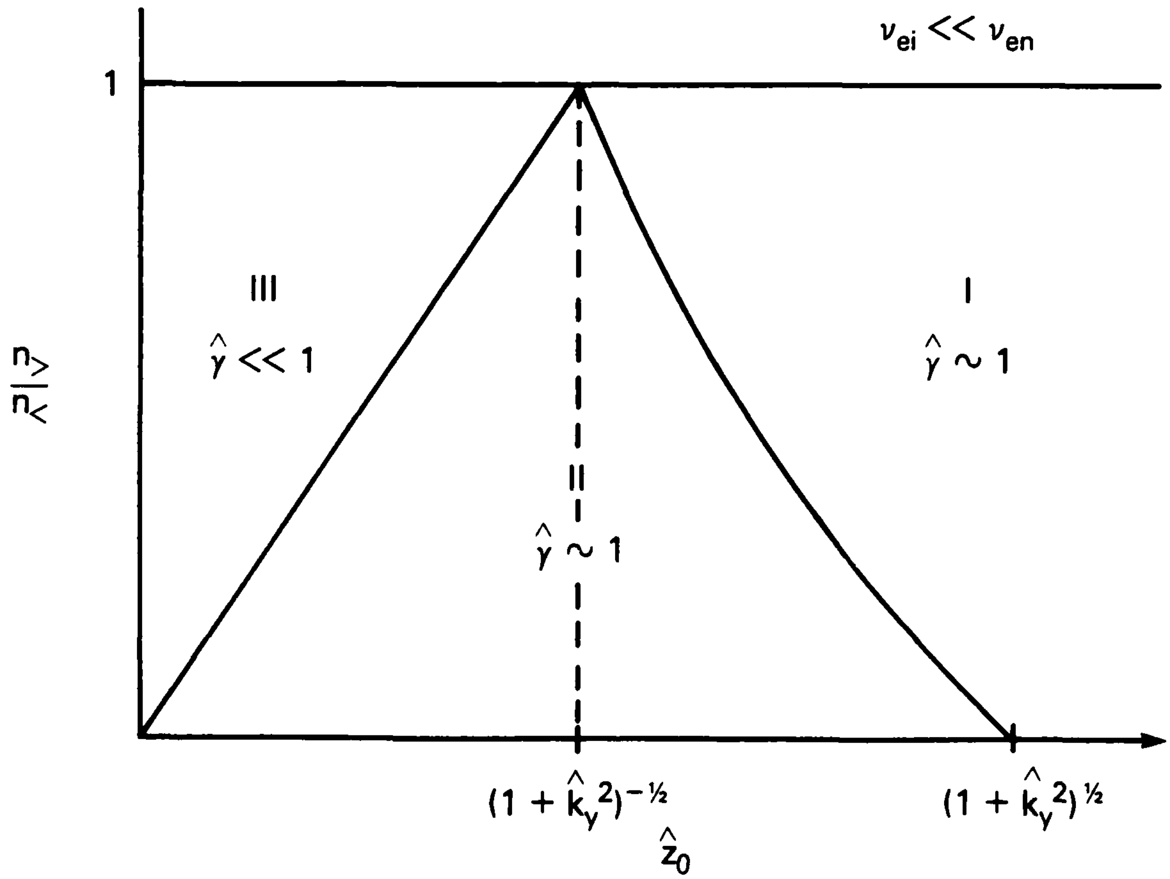

Fig. 5 Regions of validity for the growth rates in the regime $\nu_{ei} << \nu_{en}$. The growth rates are listed in Table II. This curve is similar to Fig. 2 but the boundary between regions I and II is shifted to larger $\hat{z}_0$.

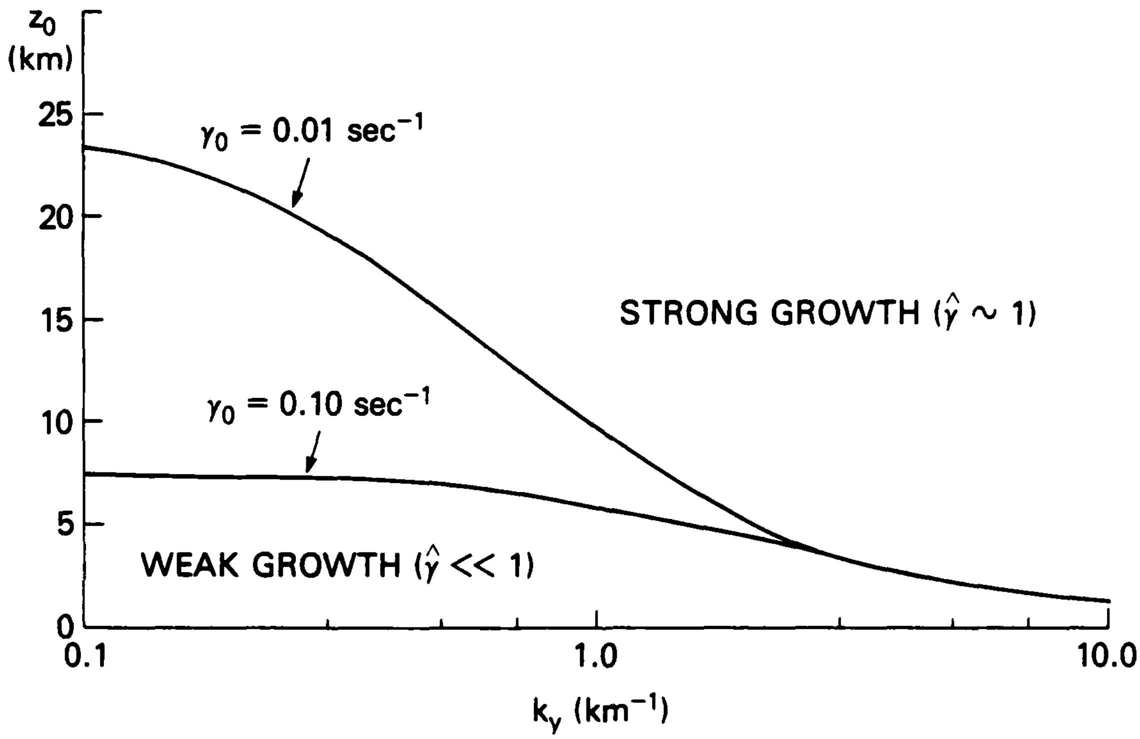

Fig. 6 Plot of "critical" parallel length $\hat{z}_{0c}$ (km) vs. perpendicular wavenumber $\hat{k}_y$ (km^{-1}) based upon (43) for typical ionospheric parameters. The parameters used are given in the text (Section IV). These curves denote the boundary between Region II [above curves - strong growth ($\hat{\gamma} \sim 1$)] and Region III [below curves - weak growth ($\hat{\gamma} << 1$)].

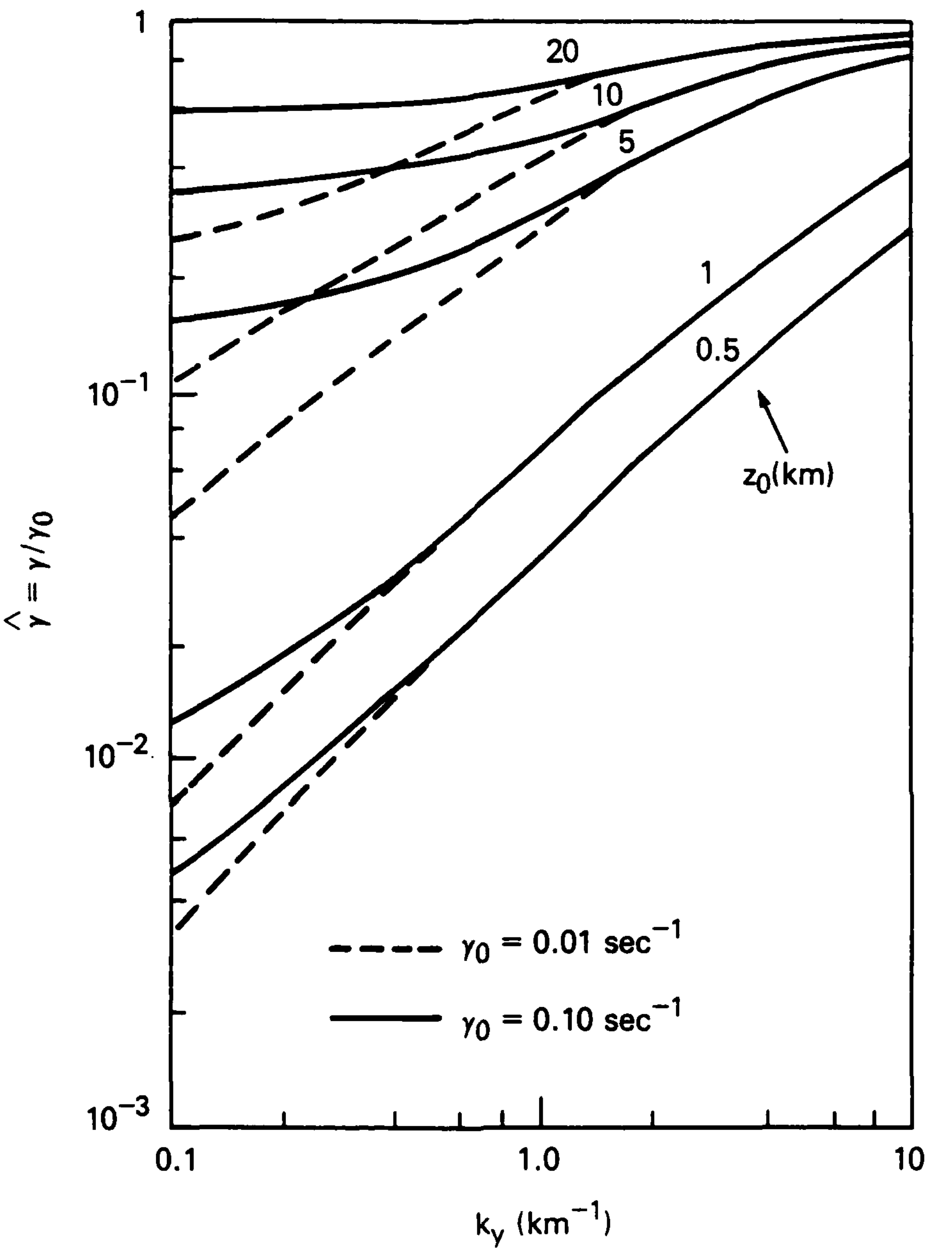

Fig. 7 Plot of perpendicular wavenumber $\hat{k}_y$ (km^{-1}) vs. growth rate $\hat{\gamma}$ (γ/γ_0) for $\gamma_0 = 0.10\ \mathrm{sec}^{-1}$ (solid curves), $\hat{\gamma}_0 = 0.01\ \mathrm{sec}^{-1}$ (dashed curves), and several values of z_0 (km). Curve is based upon (27) for $m = 0$. The ionospheric parameters used are given in the text (Section IV).

REFERENCES

Basu, B. and B. Coppi, Localized plasma depletion in the ionosphere and the equatorial spread F, Geophys. Res. Lett., 10, 900, 1983.

Braginskii, S.I., Transport processes in plasmas, in Reviews of Plasma Physics, Vol. 1, edited by M.A. Leontovich, Consultants Bureau, New York, 1965.

Chu, C., M.-S. Chu, and T. Ohkawa, Magnetostatic mode and cross-field electron transport, Phys. Rev. Lett., 41, 653, 1978.

Goldman, S.R., L. Baker, S.L. Ossakow, and A.J. Scannapieco, Striation formation associated with barium clouds in an inhomogeneous ionosphere, J. Geophys. Res., 81, 5097, 1976.

Kilb, R.W., Striation formation, in Physics of High-Altitude Nuclear Bursts, rep. DNA 4501F, Defense Nuclear Agency, Washington, D.C. 1977.

Knapp, W.S. and K. Schwartz, Aids for the study of electromagnetic blackout, rep. DNA 3499H, Defense Nuclear Agency, Washington, D.C., 1975, p. 8-5.

Linson, L.M. and G. Meltz, Theory of ion dynamics and morphology, in Analysis of Barium Clouds, rep. RADC-TR-72-736, ch. 5, Vol. 1, Avco Everett Research Laboratory, Everett, Massachusetts, 1972.

Linson, L.M. and J.B. Workman, Formation of striations in ionospheric plasma clouds, J. Geophys. Res., 75, 3211, 1970.

McDonald, B.E., M.J. Keskinen, S.L. Ossakow, and S.T. Zalesak, Computer simulation of gradient drift instability processes in Operation Avefria, J. Geophys. Res., 85, 2143, 1980.

McDonald, B.E., S.L. Ossakow, S.T. Zalesak, and N.J. Zabusky, Scale sizes and lifetimes of F region plasma cloud striations as determined by the condition of marginal stability, J. Geophys. Res., 86, 5775, 1981.

Ossakow, S.L., S.T. Zalesak, B.E. McDonald, and P.K. Chaturvedi, Nonlinear equatorial spread F: Dependence on altitude of the F peak and bottomside background electron density gradient scale length, J. Geophys. Res., 84, 17, 1979.

Ott, E., Theory of Rayleigh-Taylor bubbles in the equatorial ionosphere, J. Geophys. Res., 83, 2066, 1978.

Scannapieco, A.J. and S.L. Ossakow, Nonlinear equatorial spread F, Geophys. Res. Lett., 3, 451, 1976.

Simon, A., Instability of a partially ionized plasma in crossed electric and magnetic fields, Phys. Fluids, 6, 382, 1963.

Sperling, J.L., Role of Rayleigh-Taylor instabilities on prompt striation evolution, J. Geophys. Res., 87, 10514, 1982.

Sperling, J.L., On the effect of finite, field-aligned plasma length on a loss-cone instability, J. Geophys. Res., 88, 927, 1983.

Sperling, J.L., Finite parallel wavelengths and ionospheric structuring, J. Geophys. Res., 88, 4075, 1983.

Sperling, J.L., The evanescence of striation parameters along the geomagnetic field, J. Geophys. Res., 89, 1984 (to be published).

Sperling, J.L. and A.J. Glassman, Striation eigenmodes along the geomagnetic field and eigenvalues in the limit of strong ion-neutral collisions, JAYCOR Report J530-83-135, JAYCOR, San Diego, California, 1983.

Zalesak, S.T. and S.L. Ossakow, Nonlinear equatorial spread F: Spatially large bubbles resulting from large horizontal scale initial perturbations, J. Geophys. Res., 85, 2131, 1980.

DISTRIBUTION LIST

DEPARTMENT OF DEFENSE

ASSISTANT SECRETARY OF DEFENSE
COMM, CMD, CONT 7 INTELL
WASHINGTON, D.C. 20301

DIRECTOR
COMMAND CONTROL TECHNICAL CENTER
PENTAGON RM BE 685
WASHINGTON, D.C. 20301
01CY ATTN C-650
01CY ATTN C-312 R. MASON

DIRECTOR
DEFENSE ADVANCED RSCH PROJ AGENCY
ARCHITECT BUILDING
1400 WILSON BLVD.
ARLINGTON, VA. 22209
01CY ATTN NUCLEAR MONITORING RESEARCH
01CY ATTN STRATEGIC TECH OFFICE

DEFENSE COMMUNICATION ENGINEER CENTER
1860 WIEHLE AVENUE
RESTON, VA. 22090
01CY ATTN CODE R410
01CY ATTN CODE R812

DEFENSE TECHNICAL INFORMATION CENTER
CAMERON STATION
ALEXANDRIA, VA. 22314
02CY

DIRECTOR
DEFENSE NUCLEAR AGENCY
WASHINGTON, D.C. 20305
01CY ATTN STVL
04CY ATTN TITL
01CY ATTN DDST
03CY ATTN RAAE

COMMANDER
FIELD COMMAND
DEFENSE NUCLEAR AGENCY
KIRTLAND, AFB, NM 87115
01CY ATTN FCPR

DEFENSE NUCLEAR AGENCY
SAO/DNA
BUILDING 20676
KIRTLAND AFB, NM 87115
01CY D.C. THORNBURG

DIRECTOR
INTERSERVICE NUCLEAR WEAPONS SCHOOL
KIRTLAND AFB, NM 87115
01CY ATTN DOCUMENT CONTROL

JOINT CHIEFS OF STAFF
WASHINGTON, D.C. 20301
01CY ATTN J-3 WWMCCS EVALUATION OFFICE

DIRECTOR
JOINT STRAT TGT PLANNING STAFF
OFFUTT AFB
OMAHA, NB 68113
01CY ATTN JLTW-2
01CY ATTN JPST G. GOETZ

CHIEF
LIVERMORE DIVISION FLD COMMAND DNA
DEPARTMENT OF DEFENSE
LAWRENCE LIVERMORE LABORATORY
P.O. BOX 808
LIVERMORE, CA 94550
01CY ATTN FCPRL

COMMANDANT
NATO SCHOOL (SHAPE)
APO NEW YORK 09172
01CY ATTN U.S. DOCUMENTS OFFICER

UNDER SECY OF DEF FOR RSCH & ENGRG
DEPARTMENT OF DEFENSE
WASHINGTON, D.C. 20301
01CY ATTN STRATEGIC & SPACE SYSTEMS (OS)

WWMCCS SYSTEM ENGINEERING ORG
WASHINGTON, D.C. 20305
01CY ATTN R. CRAWFORD

COMMANDER/DIRECTOR
ATMOSPHERIC SCIENCES LABORATORY
U.S. ARMY ELECTRONICS COMMAND
WHITE SANDS MISSILE RANGE, NM 88002
01CY ATTN DELAS-EO, F. NILES

DIRECTOR
BMD ADVANCED TECH CTR
HUNTSVILLE OFFICE
P.O. BOX 1500
HUNTSVILLE, AL 35807
  01CY ATTN ATC-T MELVIN T. CAPPS
  01CY ATTN ATC-O W. DAVIES
  01CY ATTN ATC-R DON RUSS

PROGRAM MANAGER
BMD PROGRAM OFFICE
5001 EISENHOWER AVENUE
ALEXANDRIA, VA 22333
  01CY ATTN DACS-BMT J. SHEA

CHIEF C-E- SERVICES DIVISION
U.S. ARMY COMMUNICATIONS CMD
PENTAGON RM 1B269
WASHINGTON, D.C. 20310
  01CY ATTN C- E-SERVICES DIVISION

COMMANDER
FRADCOM TECHNICAL SUPPORT ACTIVITY
DEPARTMENT OF THE ARMY
FORT MONMOUTH, N.J. 07703
  01CY ATTN DRSEL-NL-RD H. BENNET
  01CY ATTN DRSEL-PL-ENV H. BOMKE
  01CY ATTN J.E. QUIGLEY

COMMANDER
U.S. ARMY COMM-ELEC ENGRG INSTAL AGY
FT. HUACHUCA, AZ 85613
  01CY ATTN CCC-EMEO GEORGE LANE

COMMANDER
U.S. ARMY FOREIGN SCIENCE & TECH CTR
220 7TH STREET, NE
CHARLOTTESVILLE, VA 22901
  01CY ATTN DRXST-SD

COMMANDER
U.S. ARMY MATERIAL DEV & READINESS CMD
5001 EISENHOWER AVENUE
ALEXANDRIA, VA 22333
  01CY ATTN DRCLDC J.A. BENDER

COMMANDER
U.S. ARMY NUCLEAR AND CHEMICAL AGENCY
7500 BACKLICK ROAD
BLDG 2073
SPRINGFIELD, VA 22150
  01CY ATTN LIBRARY

DIRECTOR
U.S. ARMY BALLISTIC RESEARCH
LABORATORY
ABERDEEN PROVING GROUND, MD 21005
  01CY ATTN TECH LIBRARY,
  EDWARD BAICY

COMMANDER
U.S. ARMY SATCOM AGENCY
FT. MONMOUTH, NJ 07703
  01CY ATTN DOCUMENT CONTROL

COMMANDER
U.S. ARMY MISSILE INTELLIGENCE AGENCY
REDSTONE ARSENAL, AL 35809
  01CY ATTN JIM GAMBLE

DIRECTOR
U.S. ARMY TRADOC SYSTEMS ANALYSIS
ACTIVITY
WHITE SANDS MISSILE RANGE, NM 88002
  01CY ATTN ATAA-SA
  01CY ATTN TCC/F. PAYAN JR.
  01CY ATTN ATTA-TAC LTC J. HESSE

COMMANDER
NAVAL ELECTRONIC SYSTEMS COMMAND
WASHINGTON, D.C. 20360
  01CY ATTN NAVALEX 034 T. HUGHES
  01CY ATTN PME 117
  01CY ATTN PME 117-T
  01CY ATTN CODE 5011

COMMANDING OFFICER
NAVAL INTELLIGENCE SUPPORT CTR
4301 SUITLAND ROAD, BLDG. 5
WASHINGTON, D.C. 20390
  01CY ATTN MR. DUBBIN STIC 12
  01CY ATTN NISC-50
  01CY ATTN CODE 5404 J. GALET

COMMANDER
NAVAL OCCEAN SYSTEMS CENTER
SAN DIEGO, CA 92152
  01CY ATTN J. FERGUSON

NAVAL RESEARCH LABORATORY
WASHINGTON, D.C. 20375
  01CY ATTN CODE 4700 S. L. Ossakow
        26 CYS IF UNCLASS. 1 CY
        IF CLASS)
  01CY ATTN CODE 4701 I Vitkovitsky
  01CY ATTN CODE 4780 J. Huba (100
        CYS IF UNCLASS, 1 CY IF CLASS)
  01CY ATTN CODE 7500
  01CY ATTN CODE 7550
  01CY ATTN CODE 7580
  01CY ATTN CODE 7551
  01CY ATTN CODE 7555
  01CY ATTN CODE 4730 E. MCLEAN
  01CY ATTN CODE 4108
  01CY ATTN CODE 4730 B. RIPIN
  20CY ATTN CODE 2628

COMMANDER
NAVAL SEA SYSTEMS COMMAND
WASHINGTON, D.C. 20362
  01CY ATTN CAPT R. PITKIN

COMMANDER
NAVAL SPACE SURVEILLANCE SYSTEM
DAHLGREN, VA 22448
  01CY ATTN CAPT J.H. BURTON

OFFICER-IN-CHARGE
NAVAL SURFACE WEAPONS CENTER
WHITE OAK, SILVER SPRING, MD 20910
  01CY ATTN CODE F31

DIRECTOR
STRATEGIC SYSTEMS PROJECT OFFICE
DEPARTMENT OF THE NAVY
WASHINGTON, D.C. 20376
  01CY ATTN NSP-2141
  01CY ATTN NSSP-2722 FRED WIMBERLY

COMMANDER
NAVAL SURFACE WEAPONS CENTER
DAHLGREN LABORATORY
DAHLGREN, VA 22448
  01CY ATTN CODE DF-14 R. BUTLER

OFFICER OF NAVAL RESEARCH
ARLINGTON, VA 22217
  01CY ATTN CODE 465
  01CY ATTN CODE 461
  01CY ATTN CODE 402
  01CY ATTN CODE 420
  01CY ATTN CODE 421

COMMANDER
AEROSPACE DEFENSE COMMAND/DC
DEPARTMENT OF THE AIR FORCE
ENT AFB, CO 80912
  01CY ATTN DC MR. LONG

COMMANDER
AEROSPACE DEFENSE COMMAND/XPD
DEPARTMENT OF THE AIR FORCE
ENT AFB, CO 80912
  01CY ATTN XPDQQ
  01CY ATTN XP

AIR FORCE GEOPHYSICS LABORATORY
HANSCOM AFB, MA 01731
  01CY ATTN OPR HAROLD GARDNER
  01CY ATTN LKB
        KENNETH S.W. CHAMPION
  01CY ATTN OPR ALVA T. STAIR
  01CY ATTN PHD JURGEN BUCHAU
  01CY ATTN PHD JOHN P. MULLEN

AF WEAPONS LABORATORY
KIRTLAND AFT, NM 87117
  01CY ATTN SUL
  01CY ATTN CA ARTHUR H. GUENTHER
  01CY ATTN NTYCE 1LT. G. KRAJEI

AFTAC
PATRICK AFB, FL 32925
  01CY ATTN TF/MAJ WILEY
  01CY ATTN TN

AIR FORCE AVIONICS LABORATORY
WRIGHT-PATTERSON AFB, OH 45433
  01CY ATTN AAD WADE HUNT
  01CY ATTN AAD ALLEN JOHNSON

DEPUTY CHIEF OF STAFF
RESEARCH, DEVELOPMENT, & ACQ
DEPARTMENT OF THE AIR FORCE
WASHINGTON, D.C. 20330
  01CY ATTN AFRDQ

HEADQUARTERS
ELECTRONIC SYSTEMS DIVISION
DEPARTMENT OF THE AIR FORCE
HANSCOM AFB, MA 01731
  01CY ATTN J. DEAS

HEADQUARTERS
ELECTRONIC SYSTEMS DIVISION/YSEA
DEPARTMENT OF THE AIR FORCE
HANSCOM AFB, MA 01732
  01CY ATTN YSEA

HEADQUARTERS
ELECTRONIC SYSTEMS DIVISION/DC
DEPARTMENT OF THE AIR FORCE
HANSCOM AFB, MA 01731
  01CY ATTN DCKC MAJ J.C. CLARK

COMMANDER
FOREIGN TECHNOLOGY DIVISION, AFSC
WRIGHT-PATTERSON AFB, OH 45433
  01CY ATTN NICD LIBRARY
  01CY ATTN ETDP B. BALLARD

COMMANDER
ROME AIR DEVELOPMENT CENTER, AFSC
GRIFFISS AFB, NY 13441
  01CY ATTN DOC LIBRARY/TSLD
  01CY ATTN OCSE V. COYNE

SAMSO/SZ
POST OFFICE BOX 92960
WORLDWAY POSTAL CENTER
LOS ANGELES, CA 90009
  (SPACE DEFENSE SYSTEMS)
  01CY ATTN SZJ

STRATEGIC AIR COMMAND/XPFS
OFFUTT AFB, NB 68113
  01CY ATTN ADWATE MAJ BRUCE BAUER
  01CY ATTN NRT
  01CY ATTN DOK CHIEF SCIENTIST

SAMSO/SK
P.O. BOX 92960
WORLDWAY POSTAL CENTER
LOS ANGELES, CA 90009
  01CY ATTN SKA (SPACE COMM SYSTEMS)
  M. CLAVIN

SAMSO/MN
NORTON AFB, CA 92409
(MINUTEMAN)
  01CY ATTN MNNL

COMMANDER
ROME AIR DEVELOPMENT CENTER, AFSC
HANSCOM AFB, MA 01731
  01CY ATTN EEP A. LORENTZEN

DEPARTMENT OF ENERGY
LIBRARY ROOM G-042
WASHINGTON, D.C. 20545
  01CY ATTN DOC CON FOR A. LABOWITZ

DEPARTMENT OF ENERGY
ALBUQUERQUE OPERATIONS OFFICE
P.O. BOX 5400
ALBUQUERQUE, NM 87115
  01CY ATTN DOC CON FOR D. SHERWOOD

EG&G, INC.
LOS ALAMOS DIVISION
P.O. BOX 809
LOS ALAMOS, NM 85544
  01CY ATTN DOC CON FOR J. BREEDLOVE

UNIVERSITY OF CALIFORNIA
LAWRENCE LIVERMORE LABORATORY
P.O. BOX 808
LIVERMORE, CA 94550
  01CY ATTN DOC CON FOR TECH INFO DEPT
  01CY ATTN DOC CON FOR L-389 R. OTT
  01CY ATTN DOC CON FOR L-31 R. HAGER

LOS ALAMOS NATIONAL LABORATORY
P.O. BOX 1663
LOS ALAMOS, NM 87545
  01CY ATTN DOC CON FOR J. WOLCOTT
  01CY ATTN DOC CON FOR R.F. TASCHEK
  01CY ATTN DOC CON FOR E. JONES
  01CY ATTN DOC CON FOR J. MALIK
  01CY ATTN DOC CON FOR R. JEFFRIES
  01CY ATTN DOC CON FOR J. ZINN
  01CY ATTN DOC CON FOR P. KEATON
  01CY ATTN DOC CON FOR D. WESTERVELT
  01CY ATTN D. SAPPENFIELD

SANDIA LABORATORIES
P.O. BOX 5800
ALBUQUERQUE, NM 87115
  01CY ATTN DOC CON FOR W. BROWN
  01CY ATTN DOC CON FOR A. THORNBROUGH
  01CY ATTN DOC CON FOR T. WRIGHT
  01CY ATTN DOC CON FOR D. DAHLGREN
  01CY ATTN DOC CON FOR 3141
  01CY ATTN DOC CON FOR SPACE PROJECT DIV

SANDIA LABORATORIES
LIVERMORE LABORATORY
P.O. BOX 969
LIVERMORE, CA 94550
  01CY ATTN DOC CON FOR B. MURPHEY
  01CY ATTN DOC CON FOR T. COOK

OFFICE OF MILITARY APPLICATION
DEPARTMENT OF ENERGY
WASHINGTON, D.C. 20545
01CY ATTN DOC CON DR. YO SONG

OTHER GOVERNMENT

INSTITUTE FOR TELECOM SCIENCES
NATIONAL TELECOMMUNICATIONS & INFO ADMIN
BOULDER, CO 80303
01CY ATTN A. JEAN (UNCLASS ONLY)
01CY ATTN W. UTLAUT
01CY ATTN D. CROMBIE
01CY ATTN L. BERRY

NATIONAL OCEANIC & ATMOSPHERIC ADMIN
ENVIRONMENTAL RESEARCH LABORATORIES
DEPARTMENT OF COMMERCE
BOULDER, CO 80302
01CY ATTN R. GRUBB
01CY ATTN AERONOMY LAB G. REID

DEPARTMENT OF DEFENSE CONTRACTORS

AEROSPACE CORPORATION
P.O. BOX 92957
LOS ANGELES, CA 90009
01CY ATTN I. GARFUNKEL
01CY ATTN T. SALMI
01CY ATTN V. JOSEPHSON
01CY ATTN S. BOWER
01CY ATTN D. OLSEN

ANALYTICAL SYSTEMS ENGINEERING CORP
5 OLD CONCORD ROAD
BURLINGTON, MA 01803
01CY ATTN RADIO SCIENCES

AUSTIN RESEARCH ASSOC., INC.
1901 RUTLAND DRIVE
AUSTIN, TX 78758
01CY ATTN L. SLOAN
01CY ATTN R. THOMPSON

BERKELEY RESEARCH ASSOCIATES, INC.
P.O. BOX 983
BERKELEY, CA 94701
01CY ATTN J. WORKMAN
01CY ATTN C. PRETTIE
01CY ATTN S. BRECHT

BOEING COMPANY, THE
P.O. BOX 3707
SEATTLE, WA 98124
01CY ATTN G. KEISTER
01CY ATTN D. MURRAY
01CY ATTN G. HALL
01CY ATTN J. KENNEY

CHARLES STARK DRAPER LABORATORY, INC.
555 TECHNOLOGY SQUARE
CAMBRIDGE, MA 02139
01CY ATTN D.B. COX
01CY ATTN J.P. GILMORE

COMSAT LABORATORIES
LINTHICUM ROAD
CLARKSBURG, MD 20734
01CY ATTN G. HYDE

CORNELL UNIVERSITY
DEPARTMENT OF ELECTRICAL ENGINEERING
ITHACA, NY 14850
01CY ATTN D.T. FARLEY, JR.

ELECTROSPACE SYSTEMS, INC.
BOX 1359
RICHARDSON, TX 75080
01CY ATTN H. LOGSTON
01CY ATTN SECURITY (PAUL PHILLIPS)

EOS TECHNOLOGIES, INC.
606 Wilshire Blvd.
Santa Monica, Calif 90401
01CY ATTN C.B. GABBARD
01CY ATTN R. LELEVIER

ESL, INC.
495 JAVA DRIVE
SUNNYVALE, CA 94086
01CY ATTN J. ROBERTS
01CY ATTN JAMES MARSHALL

GENERAL ELECTRIC COMPANY
SPACE DIVISION
VALLEY FORGE SPACE CENTER
GODDARD BLVD KING OF PRUSSIA
P.O. BOX 8555
PHILADELPHIA, PA 19101
01CY ATTN M.H. BORTNER SPACE SCI LAB

GENERAL ELECTRIC COMPANY
P.O. BOX 1122
SYRACUSE, NY 13201
01CY ATTN F. REIBERT

GENERAL ELECTRIC TECH SERVICES
  CO., INC.
HMES
COURT STREET
SYRACUSE, NY 13201
  01CY ATTN G. MILLMAN

GEOPHYSICAL INSTITUTE
UNIVERSITY OF ALASKA
FAIRBANKS, AK 99701
  (ALL CLASS ATTN: SECURITY OFFICER)
  01CY ATTN T.N. DAVIS (UNCLASS ONLY)
  01CY ATTN TECHNICAL LIBRARY
  01CY ATTN NEAL BROWN (UNCLASS ONLY)

GTE SYLVANIA, INC.
ELECTRONICS SYSTEMS GRP-EASTERN DIV
77 A STREET
NEEDHAM, MA 02194
  01CY ATTN DICK STEINHOF

HSS, INC.
2 ALFRED CIRCLE
BEDFORD, MA 01730
  01CY ATTN DONALD HANSEN

ILLINOIS, UNIVERSITY OF
107 COBLE HALL
150 DAVENPORT HOUSE
CHAMPAIGN, IL 61820
  (ALL CORRES ATTN DAN MCCLELLAND)
  01CY ATTN K. YEH

INSTITUTE FOR DEFENSE ANALYSES
1801 NO. BEAUREGARD STREET
ALEXANDRIA, VA 22311
  01CY ATTN J.M. AEIN
  01CY ATTN ERNEST BAUER
  01CY ATTN HANS WOLFARD
  01CY ATTN JOEL BENGSTON

INTL TEL & TELEGRAPH CORPORATION
500 WASHINGTON AVENUE
NUTLEY, NJ 07110
  01CY ATTN TECHNICAL LIBRARY

JAYCOR
11011 TORREYANA ROAD
P.O. BOX 85154
SAN DIEGO, CA 92138
  01CY ATTN J.L. SPERLING

JOHNS HOPKINS UNIVERSITY
APPLIED PHYSICS LABORATORY
JOHNS HOPKINS ROAD
LAUREL, MD 20810
  01CY ATTN DOCUMENT LIBRARIAN
  01CY ATTN THOMAS POTEMRA
  01CY ATTN JOHN DASSOULAS

KAMAN SCIENCES CORP
P.O. BOX 7463
COLORADO SPRINGS, CO 80933
  01CY ATTN T. MEAGHER

KAMAN TEMPO-CENTER FOR ADVANCED
STUDIES
816 STATE STREET (P.O DRAWER QQ)
SANTA BARBARA, CA 93102
  01CY ATTN DASIAC
  01CY ATTN WARREN S. KNAPP
  01CY ATTN WILLIAM MCNAMARA
  01CY ATTN B. GAMBILL

LINKABIT CORP
10453 ROSELLE
SAN DIEGO, CA 92121
  01CY ATTN IRWIN JACOBS

LOCKHEED MISSILES & SPACE CO., INC
P.O. BOX 504
SUNNYVALE, CA 94088
  01CY ATTN DEPT 60-12
  01CY ATTN D.R. CHURCHILL

LOCKHEED MISSILES & SPACE CO., INC.
3251 HANOVER STREET
PALO ALTO, CA 94304
  01CY ATTN MARTIN WALT DEPT 52-12
  01CY ATTN W.L. IMHOF DEPT 52-12
  01CY ATTN RICHARD G. JOHNSON
    DEPT 52-12
  01CY ATTN J.B. CLADIS DEPT 52-12

MARTIN MARIETTA CORP
ORLANDO DIVISION
P.O. BOX 5837
ORLANDO, FL 32805
  01CY ATTN R. HEFFNER

M.I.T. LINCOLN LABORATORY
P.O. BOX 73
LEXINGTON, MA 02173
  01CY ATTN DAVID M. TOWLE
  01CY ATTN L. LOUGHLIN
  01CY ATTN D. CLARK

MCDONNEL DOUGLAS CORPORATION
5301 BOLSA AVENUE
HUNTINGTON BEACH, CA 92647
01CY ATTN N. HARRIS
01CY ATTN J. MOULE
01CY ATTN GEORGE MROZ
01CY ATTN W. OLSON
01CY ATTN R.W. HALPRIN
01CY ATTN TECHNICAL LIBRARY SERVICES

MISSION RESEARCH CORPORATION
735 STATE STREET
SANTA BARBARA, CA 93101
01CY ATTN P. FISCHER
01CY ATTN W.F. CREVIER
01CY ATTN STEVEN L. GUTSCHE
01CY ATTN R. BOGUSCH
01CY ATTN R. HENDRICK
01CY ATTN RALPH KILB
01CY ATTN DAVE SOWLE
01CY ATTN F. FAJEN
01CY ATTN M. SCHEIBE
01CY ATTN CONRAD L. LONGMIRE
01CY ATTN B. WHITE
01CY ATTN R. STAGAT

MISSION RESEARCH CORP.
1720 RANDOLPH ROAD, S.E.
ALBUQUERQUE, NEW MEXICO 87106
01CY R. STELLINGWERF
01CY M. ALME
01CY L. WRIGHT

MITRE CORPORATION, THE
P.O. BOX 208
BEDFORD, MA 01730
01CY ATTN JOHN MORGANSTERN
01CY ATTN G. HARDING
01CY ATTN C.E. CALLAHAN

MITRE CORP
WESTGATE RESEARCH PARK
1820 DOLLY MADISON BLVD
MCLEAN, VA 22101
01CY ATTN W. HALL
01CY ATTN W. FOSTER

PACIFIC-SIERRA RESEARCH CORP
12340 SANTA MONICA BLVD.
LOS ANGELES, CA 90025
01CY ATTN E.C. FIELD, JR.

PENNSYLVANIA STATE UNIVERSITY
IONOSPHERE RESEARCH LAB
318 ELECTRICAL ENGINEERING EAST
UNIVERSITY PARK, PA 16802
(NO CLASS TO THIS ADDRESS)
01CY ATTN IONOSPHERIC RESEARCH LAB

PHOTOMETRICS, INC.
4 ARROW DRIVE
WOBURN, MA 01801
01CY ATTN IRVING L. KOFSKY

PHYSICAL DYNAMICS, INC.
P.O. BOX 3027
BELLEVUE, WA 98009
01CY ATTN E.J. FREMOUW

PHYSICAL DYNAMICS, INC.
P.O. BOX 10367
OAKLAND, CA 94610
ATTN A. THOMSON

R & D ASSOCIATES
P.O. BOX 9695
MARINA DEL REY, CA 90291
01CY ATTN FORREST GILMORE
01CY ATTN WILLIAM B. WRIGHT, JR.
01CY ATTN WILLIAM J. KARZAS
01CY ATTN H. ORY
01CY ATTN C. MACDONALD
01CY ATTN R. TURCO
01CY ATTN L. DeRAND
01CY ATTN W. TSAI

RAND CORPORATION, THE
1700 MAIN STREET
SANTA MONICA, CA 90406
01CY ATTN CULLEN CRAIN
01CY ATTN ED BEDROZIAN

RAYTHEON CO.
528 BOSTON POST ROAD
SUDBURY, MA 01776
01CY ATTN BARBARA ADAMS

RIVERSIDE RESEARCH INSTITUTE
330 WEST 42nd STREET
NEW YORK, NY 10036
01CY ATTN VINCE TRAPANI

SCIENCE APPLICATIONS, INC.
1150 PROSPECT PLAZA
LA JOLLA, CA 92037
01CY ATTN LEWIS M. LINSON
01CY ATTN DANIEL A. HAMLIN
01CY ATTN E. FRIEMAN
01CY ATTN E.A. STRAKER
01CY ATTN CURTIS A. SMITH

SCIENCE APPLICATIONS, INC
1710 GOODRIDGE DR.
MCLEAN, VA 22102
01CY J. COCKAYNE
01CY E. HYMAN

SRI INTERNATIONAL
333 RAVENSWOOD AVENUE
MENLO PARK, CA 94025
01CY ATTN J. CASPER
01CY ATTN DONALD NEILSON
01CY ATTN ALAN BURNS
01CY ATTN G. SMITH
01CY ATTN R. TSUNODA
01CY ATTN DAVID A. JOHNSON
01CY ATTN WALTER G. CHESNUT
01CY ATTN CHARLES L. RINO
01CY ATTN WALTER JAYE
01CY ATTN J. VICKREY
01CY ATTN RAY L. LEADABRAND
01CY ATTN G. CARPENTER
01CY ATTN G. PRICE
01CY ATTN R. LIVINGSTON
01CY ATTN V. GONZALES
01CY ATTN D. MCDANIEL

TECHNOLOGY INTERNATIONAL CORP
75 WIGGINS AVENUE
BEDFORD, MA 01730
01CY ATTN W.P. BOQUIST

TOYON RESEARCH CO.
P.O. Box 6890
SANTA BARBARA, CA 93111
01CY ATTN JOHN ISE, JR.
01CY ATTN JOEL GARBARINO

TRW DEFENSE & SPACE SYS GROUP
ONE SPACE PARK
REDONDO BEACH, CA 90278
01CY ATTN R. K. PLEBUCH
01CY ATTN S. ALTSCHULER
01CY ATTN D. DEE
01CY ATTN D/ STOCKWELL
SNTF/1575

VISIDYNE
SOUTH BEDFORD STREET
BURLINGTON, MASS 01803
01CY ATTN W. REIDY
01CY ATTN J. CARPENTER
01CY ATTN C. HUMPHREY

UNIVERSITY OF PITTSBURGH
PITTSBURGH, PA 15213
01CY ATTN: N. ZABUSKY

END

FILMED

11-84

DTIC